

ROLE OF FLUID TRANSPORT ON SEALING EFFECTIVENESS OF AIR CURTAINS

TANMAY AGRAWAL



**DEPARTMENT OF APPLIED MECHANICS
INDIAN INSTITUTE OF TECHNOLOGY DELHI
SEPTEMBER 2025**

© Indian Institute of Technology Delhi (IITD), New Delhi, 2025

Role of fluid transport on sealing effectiveness of air
curtains

by

Tanmay Agrawal

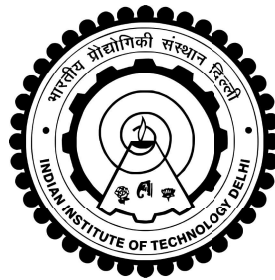
Department of Applied Mechanics

Submitted

In fulfillment of the requirements of the degree of

Doctor of Philosophy

to the



INDIAN INSTITUTE OF TECHNOLOGY DELHI

September, 2025

Certificate

This is to certify that the thesis entitled “**Role of fluid transport on sealing effectiveness of air curtains**”, submitted by **Mr. Tanmay Agrawal** to the **Indian Institute of Technology Delhi** for the award of the degree of **Doctor of Philosophy** is a record of the original, bona fide research work carried out by him under our supervision. The thesis works meets the requisite standards and the candidate is worthy of consideration for the degree of Doctor of Philosophy in accordance with the regulations of the institute.

The results contained in this thesis have not been submitted in part or in full to any other university or institute for the award of any degree or diploma.

Dr. Narsing K. Jha
Assistant Professor
Department of Applied Mechanics,
Indian Institute of Technology Delhi
Hauz Khas, New Delhi, India - 110016

Dr. Vamsi K. Chalamalla
Associate Professor
Department of Applied Mechanics,
Indian Institute of Technology Delhi
Hauz Khas, New Delhi, India - 110016

ACKNOWLEDGEMENTS

Though the front page of this document bears a single name, its manifestation from a vague idea to scientifically exciting findings has been possible only through the consistent support of many individuals. First and foremost, I would like to thank my supervisors, Prof. Narsing Kumar Jha and Prof. Vamsi Krishna Chalamalla, for guiding me throughout my PhD journey. Their individual expertise in experiments and computations, respectively, is the only reason this thesis could offer combined insights from both laboratory measurements and numerical simulations. I consider myself very fortunate to have learned from their dynamic personalities, which continually inspired me to pursue a deeper, more rigorous, and thorough understanding of fluid mechanics. They provided the creative freedom for my wild ideas to take shape, and subsequently, as a *Guru*, nurtured my technical and personal development. From our online meetings during the second wave of the COVID outbreak to the marathon discussions on the lesser-understood aspects of stratified and environmental flows, they helped me develop critical thinking skills and perspectives I would not have otherwise attained. Through their wisdom, I learned how to ask the right questions and how to approach them thoughtfully, while remaining critical of the process. I am optimistic that our collaboration will extend beyond my PhD, and I look forward to opportunities to work together on a wider variety of fluid dynamics problems.

I have had the fortune of having an extremely knowledgeable, approachable, and humble research committee. The committee chair, Prof. Anupam Dewan, provided valuable feedback during annual reviews as well as in personal interactions, drawing from his extensive experience in computational studies of turbulent jets. During my initial days at IIT, his book on tackling turbulence through numerical techniques greatly helped me gain a fundamental understanding of LES and RANS. The internal expert of my research committee, Prof. Amitabh Bhattacharya, always welcomed my questions with a warm smile and offered important considerations for both experiments and simulations. His approach to problem-solving and critical thinking has continuously inspired me throughout my candidature. I am also grateful to Prof. Krishnakant Agrawal, the external expert, whose suggestions from a practical standpoint, likely informed by his years of industrial and academic experience, were crucial in improving the overall quality of this thesis. In addition to them, I am sincerely thankful to the anonymous referees whose comments added significant value to this thesis. It is due to them if you'll appreciate the readability of this document.

The work presented in this thesis would not have been possible without the support of various funding agencies over the years. First and foremost, I have had the honor of being a Prime Minister's Research Fellow (PMRF), for which I express my deep gratitude to the Ministry of Education, Government of India. The Indian Government also supported my PhD candidature through the MHRD fellowship for the remainder of my time at IIT Delhi when I was no longer receiving PMRF support. I am also thankful for the International Travel Support (ITS) from the Science & Engineering Research Board (SERB), which enabled me to travel to Cambridge, UK, to attend a summer school that significantly contributed to my learning and academic network. The conference travel award from IRD, IIT Delhi, is also gratefully acknowledged that enabled traveling to Germany to attend the

EFDC conference which provided meaningful networking opportunities.

The experiments you will read about in this thesis required a much larger contribution than the author alone. Throughout different measurement campaigns, I had the privilege of being accompanied by many helpful and sincere colleagues. For the experiments on measuring the sealing effectiveness of neutrally buoyant and heavy air curtains, Shresth and Ayank actively helped during and after the measurements. The analytical model developed for heavy air curtains is largely due to the clever thinking and perseverance of Shresth. In PIV measurements, I had the fortune of being assisted by Amrit and Satyarth, who painstakingly conducted multiple repetitions of a single experiment to obtain a satisfactory ensemble. Amrit's effort toward the fabrication and testing of the rectangular nozzle to ensure a plane jet is deeply appreciated. The earlier iterations of this nozzle were made possible due to Dinesh Sir and Madan Sir, who spent substantial time on their lathes and milling machines for the demanding fabrication. While last, but definitely not least, the staff of the Fluid Mechanics Laboratory (133A) were very kind in offering their support. Yogesh Sir in particular, who not only provided his technical insights on various matters but also greatly helped with administrative tasks, thereby making my academic journey easier. Jaiprakash Ji and Sunil helped throughout the measurement phase by offering their creative craftsmanship.

The data from the numerical simulations played a crucial role throughout my PhD. To this end, I would wholeheartedly thank the development team behind SOMAR, who must have spent countless hours developing and optimizing the code. I am particularly grateful to Dr. Ed Santilli, who supervised and personally assisted during the initial implementation and debugging of the source code for adaptation to simulate air curtain flows. The spatiotemporal data generated from SOMAR equipped me with sufficient numbers to crunch

for the analysis presented in this thesis. Throughout my candidature, several other students in the department were involved in flow simulations and offered their insights. Most notably, discussions with Diptanu Das, who studied buoyant air curtains using RANS for his MSR thesis, advanced my physical understanding of the buoyancy effects in an ACD.

Towards data processing and developing a deeper understanding of buoyancy-driven turbulent flows, I have had fruitful discussions with colleagues, both past and present, who deserve special mention. Dr. Siva Heramb Peddada (Siva Garu) and Dr. Nitin Kumar (Badka Ji) have been invaluable in conducting simulations, analyzing results, and interpreting computational data. I have also greatly benefited from discussions with my former colleagues, Dr. Rahul Deshpande and Dr. Tushar Sikroria, who, at various times, have nudged me in the right direction. Rahul's timely advice on data analysis, along with Tushar's insights on PIV, saved me a great deal of time I would have otherwise spent searching through the internet. I would also thank Dr. Bhaarath Ramesh, with whom I have had many technical and non-technical telephonic conversations, which filled me with a sense of joy and calmness.

While it is generally conceived that a PhD journey is highly academic (which it is), it need not be monotonous. I have been fortunate to avoid that aspect thanks to a wonderful group of friends with whom I have shared countless moments over great food and drinks. Not surprisingly, many of them are my lab mates, with whom my collaboration extended far beyond academics. In no particular order, I had the company of Arnab, Niladri, Sitaram, Suraj, Vamsi, Bhramar, Manoj, Divyaprakash, Srihari, Datti, Amrat, Shoaib, Prantik, Shivam, Varnit, Subrat, Deepshikha, Pratyush, and Amar over food, cricket, badminton, and outings. During my time at Kumaon Hostel, the memories created with Drs. Shubham Dubey, Krishna Gola, and Ashutosh Negi, and juniors including Aman, Jatin, Rohit, Harsh, Prayag, Rishabh, Himanshu, Dharamjeet, and Milind will always be cher-

ished for years to come. Away from home, I had the kind acceptance of my colleague Shishir bhaiya (Dr. Sahab) and his family, who were always there to provide hearty meals whether I was healthy or sick, and to offer support and encouragement throughout my academic progress. I look forward to Swastik's (their child's) wonderful future.

Although it is conventional to acknowledge family towards the end, none of this would exist without the support of my strongest pillars to whom this work is dedicated. Despite challenging life situations, my mother, sister and grandfather always encouraged my research, likely at the expense of their own happiness and contentment. It would be impossible for me to fully express their sacrifices, unspoken words, and countless prayers for the completion of my PhD. I am grateful, from the deepest core of my heart, for their selfless love and understanding, and I seek forgiveness for the times I may not have been there when they needed me. My wife, Anjali, has shared her love, affection, and unwavering care across every aspect of my personal and academic life. In countless situations, she has been my guiding light, offering the support I needed to navigate the challenges of work-life balance. Throughout this journey, she has been my anchor who steadily safeguarded my mental well-being and taught me the importance of empathy toward others which I usually lack. While I'm not proud that she often bears the brunt of my frustrations and anguish, she remains my greatest inspiration in striving for higher ideals, both academically and as a human being. Her constant presence through the highs and lows of my PhD has been universally irreplaceable, as is the assurance of support that her presence has brought me over the years. As I complete this doctoral journey, I look forward with gratitude and excitement to all the journeys we will take together. This thesis is lovingly dedicated to you.

ABSTRACT

Fluid flow across openings in buildings arises due to buoyancy forces caused by indoor-outdoor temperature differences, wind effects, and pressure gradients. These flows often lead to undesirable transport of heat, mass, contaminants, and pollutants, posing a challenge to maintaining energy-efficient, clean, and comfortable indoor environments. Heating Ventilation and Air-Conditioning (HVAC) systems are therefore forced to work harder to compensate for this unregulated exchange, resulting in increased energy consumption. One effective mitigation strategy is the use of air curtain devices (ACDs) installed on doorways, which generate a high-momentum jet that acts as an aerodynamic separation barrier and suppress the buoyancy-driven exchange while allowing uninterrupted passage through them. ACDs have been deployed in various configurations, including vertical, horizontal, twin-jet, and recirculating designs, depending on functional needs. Their performance depends on the balance between jet momentum flux and opposing buoyancy forces, captured by a non-dimensional parameter called the deflection modulus, D_m . For an optimally designed ACD, the jet inhibits gravity currents which are horizontal intrusions of buoyant fluid driven by the density difference. However, if the jet momentum is insufficient, the curtain becomes unstable, reducing its sealing effectiveness.

The present study aims to provide a deeper understanding of the flow physics governing a vertically blowing air curtain. The primary objective is to investigate the interaction between the plane jet and the opposing gravity current, examining how their interplay

affects the stability, dynamics, and overall effectiveness of the curtain. The influence of buoyancy is analyzed through comparisons with non-buoyant jets and turbulent fountains. We also assess the impact of assistive buoyancy, which is introduced by using a denser curtain fluid, on suppressing fluid infiltration. Finally, the study investigates the transport pathways through which outdoor fluid enters the indoor space, even when an air curtain is in place. These insights aim to explain the mechanisms that limit sealing performance and identify the operating conditions under which aerodynamic sealing can approach its ideal behavior.

The present study employs a combination of computational and experimental methods to investigate the dynamics of vertically blowing ACDs. Numerically, both Reynolds-averaged Navier-Stokes (RANS) and large-eddy simulation (LES) approaches are used to obtain spatiotemporal distributions of velocity and density fields, with LES performed using the high-fidelity in-house solver SOMAR for enhanced accuracy. Experimentally, time-resolved particle image velocimetry (PIV) is conducted in a refractive index-matched setup to capture temporal velocity fields. These measurements are complemented by planar flow visualizations using dye injection for qualitative assessment, and by bulk density and conductivity measurements before and after each trial to accurately quantify sealing effectiveness. Additionally, a reduced-order analytical model is developed to predict jet deflection and velocity characteristics, which are compared with the numerical data. Together, these methods offer a synergetic approach to thoroughly investigate the factors governing air curtain performance and the associated fluid transport mechanisms.

The results from this study provide a detailed analysis of air curtain behavior across various operating conditions, highlighting the critical role of deflection modulus, D_m , in determining flow stability and sealing performance. For neutrally buoyant air curtains (NBACs),

where curtain density matches the indoor environment, experimental observations and LES results confirm that the sealing effectiveness, E , is significantly low for unstable ACDs ($D_m \lesssim 0.1$) and achieves a maximum value in the vicinity of $D_m \approx 0.2$ when the curtain becomes stable. LES predictions show strong agreement with experimental values, unlike RANS, which under-predicts effectiveness due to its inherent averaging. When assisting buoyancy is introduced using denser curtain fluids, termed heavy air curtains (HACs), infiltration of outdoor fluid reduces by nearly 25% at moderate values of D_m . Dynamically similar laboratory experiments, employing sugar solution as curtain fluid and salt- and freshwater as outdoor and indoor analogs, confirm that assistive buoyancy improves performance, achieving sealing effectiveness up to 0.85. The transport mechanisms associated with the fluid which contributes to this 15% exchange and infiltrates into the indoor region through the air curtain is still not very well understood. To address this, the present study adopts a Lagrangian particle tracking method which examines the trajectories of fluid particles that migrate from the outdoor region to the indoor space. Results indicate that even under the established conditions when an ACD completely inhibits the gravity current, fluid particles are entrained into the air curtain jet and subsequently penetrate the indoor environment after impingement on the floor.

The statistical characteristics of air curtains is examined through direct comparison with non-buoyant plane jets and turbulent fountains. At moderate values of D_m , air curtains exhibit significant inclination from the vertical, resulting in distinct temporal flow evolution in indoor and outdoor regions due to buoyancy effects. Ensemble-averaged data from PIV measurements and high-fidelity LES computations reveal that ACDs exhibit asymmetric lateral spreading, particularly toward the buoyant (outdoor) side, as a consequence of jet interaction with lateral density stratification. This asymmetry is also evident in the tur-

bulence statistics, leading to deviations from the self-similar behavior typically observed in plane turbulent jets. Laboratory measurements and numerical data coherently suggests that the decay rate of centreline velocity (K_W), and the spreading rate of halfwidth (K_δ) of air curtains are higher as compared to non-buoyant jets. For fountains developing in a uniform ambient, K_W and K_δ are found to be negatively correlated with the source Froude number, Fr_0 . Furthermore, integral estimations of volume and momentum fluxes reveal that entrainment coefficients for ACDs increase by up to 20%, compared to configurations without lateral density differences. Whereas for the high- Fr_0 fountains, the fluid entrainment is similar to a non-buoyant jet.

In conclusion, this thesis presents a comprehensive analysis of air curtain dynamics under realistic buoyancy influences, integrating experimental observations with high-fidelity simulations to evaluate sealing effectiveness and characterize fluid transport. Novel insights into the general structure of air curtains and turbulent line fountains, including their velocity statistics and entrainment characteristics, are presented. To further advance this work, future studies could investigate the time-resolved evolution of instantaneous fluid transport across the turbulent/non-turbulent interface (TNTI), as well as the development of fluid instabilities on either side of the air curtain jet arising from the interaction of fluids with differing densities.

सार

भवनों में खुले स्थानों के आर-पार द्रव प्रवाह मुख्यतः इनडोर और आउटडोर तापमान में अंतर, वायु प्रभावों और दाब प्रवणताओं के कारण उत्पन्न उर्ध्वगामी बलों से होता है। ये प्रवाह प्रायः ऊष्मा, द्रव्य, प्रदूषक तथा अन्य हानिकारक तत्वों के अवांछनीय आदान-प्रदान का कारण बनते हैं, जिससे ऊर्जा-कुशल, स्वच्छ और आरामदायक इनडोर वातावरण बनाए रखना चुनौतीपूर्ण हो जाता है। इसके परिणामस्वरूप ताप, वेंटिलेशन और वातानुकूलन प्रणालियों को अधिक परिश्रम करना पड़ता है, जिससे ऊर्जा की खपत बढ़ जाती है। एक प्रभावी समाधान दरवाजों पर वायु परदों का उपयोग है, जो उच्च वेग का एक जेट प्रवाह उत्पन्न करते हैं और एक वायुगतिकीय अवरोधक के रूप में कार्य करते हुए उर्ध्वगामी प्रवाहों को रोकते हैं, साथ ही निर्बाध आवागमन की अनुमति भी देते हैं। वायु परदों को कार्यात्मक आवश्यकताओं के अनुसार लंबवत, क्षैतिज, द्वि-जेट तथा पुनर्चक्रित डिज़ाइन में स्थापित किया जाता है। इनकी कार्यक्षमता जेट के वेगीय बल और विपरीत उर्ध्वगामी बलों के बीच संतुलन पर निर्भर करती है, जिसे एक अदिमांक मानक द्वारा व्यक्त किया जाता है। यदि वायु पर्दा उपयुक्त रूप से डिज़ाइन किया गया हो, तो जेट प्रवाह गुरुत्वीय धाराओं, अर्थात् घनत्व भिन्नता से प्रेरित क्षैतिज प्रवाहों, को रोक देता है। परन्तु यदि जेट का वेग बल अपर्याप्त हो, तो पर्दा अस्थिर हो जाता है और उसकी प्रभावशीलता घट जाती है।

यह अध्ययन एक लंबवत प्रवाहित वायु पर्दे के प्रवाहीय भौतिकी को गहराई से समझने के उद्देश्य से किया गया है। इसका मुख्य उद्देश्य समतल जेट प्रवाह और विपरीत दिशा में प्रवाहित गुरुत्वीय धारा के बीच अंतःक्रिया का परीक्षण करना है तथा यह विश्लेषण करना है कि इनका आपसी प्रभाव पर्दे की स्थिरता, गतिकी और समग्र प्रभावशीलता को किस प्रकार प्रभावित करता है। अध्ययन में गैर-उर्ध्वगामी जेट प्रवाह तथा अशांत जलप्रपातों के साथ तुलना करके उर्ध्वगामी बलों के प्रभावों का भी विश्लेषण किया गया है। साथ ही, पर्दे के तरल के घनत्व को बढ़ाकर सहायक उर्ध्वगामी बल उत्पन्न करने के प्रभाव का परीक्षण किया गया है, जो बाहरी द्रव के प्रवेश को कम करने में सहायक होता है। अंत में, यह अध्ययन उन मार्गों का अन्वेषण करता है जिनसे बाहरी द्रव वायु पर्दे की उपस्थिति के बावजूद इनडोर क्षेत्र में प्रवेश करता है। यह समझ वास्तविक प्रवाह तंत्रों को स्पष्ट करने में सहायता करेगी जो पर्दे की सीलिंग प्रभावशीलता को सीमित करते हैं, तथा उन परिस्थितियों की पहचान करेगी जिनमें वायुगतिकीय सीलिंग आदर्श प्रदर्शन के निकट पहुँच सकती है।

यह अध्ययन वायु परदे की गतिकी के विश्लेषण हेतु संगणकीय तथा प्रायोगिक दोनों विधियों का उपयोग करता है। संगणकीय रूप से, पुनरावृत्त औसत नवियर-स्टोक्स समीकरणों और बड़े भंवर सिमुलेशन विधियों द्वारा वेग तथा घनत्व क्षेत्रों के स्थानिक-कालिक वितरण प्राप्त किए गए हैं। बड़े भंवर सिमुलेशन के लिए उच्च गुणवत्ता वाले आंतरिक सॉफ्टवेयर का प्रयोग किया गया है। प्रायोगिक रूप में, समय-संवेदनशील कण चित्र वेगमिति तकनीक द्वारा एक समान अपवर्तनांक वाले सेटअप में प्रवाह क्षेत्र का मापन किया गया है। इन मापों को रंग घोल प्रविष्टि द्वारा प्रवाह का दृश्यांकन कर और प्रत्येक परीक्षण से पहले तथा बाद में घनत्व और चालकता मापकर सत्यापित किया गया है। इसके अतिरिक्त, जेट विक्षेपण और वेग विशेषताओं की भविष्यवाणी हेतु एक सरल गणितीय मॉडल विकसित किया गया है, जिसकी तुलना संगणकीय परिणामों से की गई है। ये सभी विधियाँ मिलकर वायु पर्दे के प्रदर्शन तथा संबंधित द्रव परिवहन तंत्रों की व्यापक जांच प्रस्तुत करती हैं।

अध्ययन के परिणाम विभिन्न परिचालन स्थितियों में वायु परदे के व्यवहार का विस्तृत विश्लेषण प्रदान करते हैं और दिखाते हैं कि विचलन गुणांक वायु पर्दे की स्थिरता और सीमांकन क्षमता में महत्वपूर्ण भूमिका निभाता है। तटस्थ घनत्व वाले वायु पर्दों के लिए, जहाँ पर्दे का द्रव इनडोर वातावरण के घनत्व के समान होता है, प्रायोगिक अवलोकन और बड़े भंवर सिमुलेशन से यह पुष्टि हुई है कि जब विचलन गुणांक लगभग 0.1 से कम होता है तब पर्दा अस्थिर होता है और सीमांकन क्षमता बहुत कम रहती है, जबकि विचलन गुणांक लगभग 0.2 के आसपास पहुँचने पर पर्दा स्थिर हो जाता है और अधिकतम सीमांकन क्षमता प्राप्त होती है। बड़े भंवर सिमुलेशन के परिणाम प्रायोगिक मापनों से अच्छी तरह मेल खाते हैं, जबकि पुनरावृत्त औसत नवियर-स्टोक्स सिमुलेशन सीमांकन क्षमता को कम आंकते हैं। जब भारी वायु पर्दे का उपयोग किया गया, अर्थात् घनत्व बढ़ाकर सहायक उर्ध्वगामी बल डाला गया, तो लगभग 25 प्रतिशत तक बाहरी द्रव का प्रवेश कम हुआ। प्रयोगशाला प्रयोगों में चीनी घोल को पर्दे के द्रव के रूप में और नमक तथा ताजे पानी को बाहरी और इनडोर द्रव के अनुरूप उपयोग किया गया, और पाया गया कि सहायक उर्ध्वगामी बल से सीमांकन क्षमता 0.85 तक पहुँच सकती है।

हालाँकि, अभी भी लगभग 15 प्रतिशत बाहरी द्रव इनडोर क्षेत्र में प्रवेश करता है, जिसकी प्रवाह प्रक्रिया पूरी तरह से नहीं समझी गई थी। इस समस्या को हल करने के लिए, अध्ययन में लैंग्रेंजियन कण ट्रैकिंग तकनीक अपनाई गई, जिसमें उन तरल कणों की यात्रा का अध्ययन किया गया जो बाहरी क्षेत्र से इनडोर क्षेत्र में प्रवेश करते हैं। परिणाम बताते हैं कि जब वायु पर्दा गुरुत्वीय धारा को पूरी तरह रोकता है, तब भी कुछ तरल कण वायु पर्दे के जेट में सम्मिलित

होकर फर्श से टकराने के बाद इनडोर क्षेत्र में प्रवेश कर जाते हैं।

वायु पर्दों के सांख्यिकीय व्यवहार का विश्लेषण गैर-उर्ध्वगामी समतल जेट प्रवाहों और अशांत जलप्रपातों के साथ प्रत्यक्ष तुलना करके किया गया। मध्यम विचलन गुणांक मानों पर वायु परदे में ऊर्ध्वाधर दिशा से पर्याप्त झुकाव देखा गया, जिससे इनडोर और बाहरी क्षेत्रों में प्रवाह की समय के साथ अलग-अलग विकास प्रक्रिया देखी गई। समष्टि औसत आंकड़ों से पता चलता है कि वायु परदे पार्श्व दिशा में विषम प्रसार करते हैं, विशेषतः उर्ध्वगामी (बाहरी) दिशा में, जो पार्श्व घनत्व संरचनाओं के कारण उत्पन्न होता है। यह विषमता प्रवाह में अशांतता के आंकड़ों में भी प्रकट होती है, जिसके कारण वायु परदे पारंपरिक समतल अशांत जेटों में देखी जाने वाली समानता का पालन नहीं करते। प्रयोगशाला मापन और संगणकीय आंकड़े यह भी दर्शाते हैं कि वायु परदे की केंद्रेखीय वेग क्षय दर और अर्ध-चौड़ाई फैलाव दर गैर-उर्ध्वगामी जेट प्रवाहों की तुलना में अधिक होती है। एकसमान परिवेश में विकसित जलप्रपातों के लिए यह दरें स्रोत उर्ध्वगामी बलांक के साथ नकारात्मक रूप से संबंधित पाई गईं। इसके अलावा, संवेग और आयतन प्रवाह के समाकलन से पता चलता है कि वायु पर्दों के अंतर्वेशन गुणांक में लगभग 20 प्रतिशत तक वृद्धि होती है, जबकि उच्च स्रोत उर्ध्वगामी बलांक वाले जलप्रपातों में यह अंतर्वेशन गैर-उर्ध्वगामी जेट के समान रहता है।

अंततः, यह शोध वास्तविक उर्ध्वगामी प्रभावों के अधीन वायु पर्दे की गतिकी का एक समग्र विश्लेषण प्रस्तुत करता है, जो प्रायोगिक टिप्पणियों और उच्च गुणवत्ता वाले संगणकीय सिमुलेशन के समन्वय से सीमांकन क्षमता और द्रव प्रवाह की प्रकृति का मूल्यांकन करता है। वायु परदे और अशांत रेखीय जलप्रपातों की संरचना, वेग सांख्यिकी और अंतर्वेशन विशेषताओं में नवीन अंतर्दृष्टियाँ प्रस्तुत की गई हैं। भविष्य में, तात्कालिक द्रव प्रवाह के समय के साथ विकास और विभिन्न घनत्वों वाले द्रवों के बीच उत्पन्न प्रवाहीय अस्थिरताओं के अध्ययन द्वारा इस कार्य को और आगे बढ़ाया जा सकता है।

Contents

Certificate	i
ACKNOWLEDGEMENTS	ii
ABSTRACT	vii
List of figures	xvii
List of tables	xxiii
List of symbols	xxvi
List of abbreviations	xxviii
1 Introduction	1
1.1 Background and motivation	3
1.1.1 Buoyancy-driven flow	3
1.1.2 Air curtains	5
1.2 Research significance and challenges	8
1.2.1 Significance of the present work	8
1.2.2 Challenges associated with the ACD flow physics	9
1.3 Scope and Objectives	10
2 Literature Review	13
2.1 Experimental research	15
2.1.1 Foundational studies	15
2.1.2 Plane turbulent jets	18
2.1.3 Buoyancy effects in jets	21

2.1.4	Practical applications	24
2.1.4.1	Fire safety	24
2.1.4.2	Building ventilation	25
2.1.5	Research gaps	28
2.2	Numerical simulations	29
2.2.1	Early computational effort	30
2.2.2	Reynolds-averaged Navier-Stokes simulations	31
2.2.3	Large-eddy simulations	40
2.2.4	Research gaps	43
2.3	Research questions	46
2.4	Thesis outline	46
3	Neutrally buoyant air curtains	49
3.1	Numerical methodology	50
3.1.1	Reynolds-averaged Navier-Stokes	50
3.1.2	Large-eddy simulation	53
3.1.3	Computational domain and parameter space	55
3.2	Experiments	60
3.2.1	Flow facility	60
3.2.2	Dye visualisation	64
3.2.3	Effectiveness measurement	65
3.3	Data validation	68
3.3.1	Planar jet flow	68
3.3.2	Lock-exchange flow	73
3.4	Results	75
3.4.1	General flow structure	75
3.4.2	Air curtain effectiveness	78
3.4.3	Energy budget	81
4	Heavy air curtains	87
4.1	Numerical simulations	88
4.2	Experiments	92

4.2.1	Redefining air curtain effectiveness	93
4.3	Analytical model	96
4.4	Results	100
4.4.1	Dye visualization	100
4.4.2	Effectiveness estimates	103
4.4.3	Parametric effect of S	105
4.4.4	Comparison with analytical model	106
5	Velocity statistics and entrainment	111
5.1	Numerical simulations	113
5.2	Experiments	117
5.2.1	Nozzle design	121
5.2.2	PIV measurements	124
5.3	Data analysis	126
5.4	Experimental data validation	128
5.5	Results	131
5.5.1	Transient flow development	132
5.5.1.1	General structure of impinging fountains	132
5.5.1.2	Effect of lateral density difference	136
5.5.1.3	Quantification of the lateral spread	141
5.5.2	Quasi-steady description of the flow	144
5.5.2.1	Lateral deflection	145
5.5.2.2	Velocity statistics along the centerline	150
5.5.2.3	Cross-stream statistics	154
5.5.3	Quantification of turbulent entrainment	160
5.5.3.1	Establishing the integration limits	160
5.5.3.2	Integral measure of fluxes and entrainment coefficient	164
6	Lagrangian characterization of fluid transport	172
6.1	Particle trajectories	173
6.1.1	Classification	176
6.2	Characterization of transport pathways	180

6.2.1 Bulk transport of passive scalar	185
7 Discussion and conclusion	188
7.1 Main findings	189
7.2 Research impact	193
7.3 Future scope	196
References	199
Appendix A	208
Biodata	210

List of Figures

1.1	Experimental realization of a gravity current formed using freshwater (light) and saltwater (dense) obtained through shadowgraph technique. The nose of the gravity current is marked by an arrow. Taken from Britter and Simpson [1].	3
1.2	Schematic of a general air curtain installation. Subscripts d , l and θ denote properties associated with dense, light and curtain fluids. α_0 and α_f represent the initial and final angular tilt of the air curtain with respect to the vertical direction.	5
1.3	Practical implementation of air curtains in everyday life. They are installed to manage the transport of heat, pollutant, insects and dust across building openings.	6
2.1	Flowchart of the present literature review comprising experimental and numerical studies leading to the formulation of research questions.	14
2.2	Laser visualization of the air curtain, theoretical and experimental jet bending at null mean flow conditions. Taken from Guyonnaud et al. [2]	18
2.3	(a) Instantaneous velocity magnitude (normalised) in the developing region, and (b) dimensionless time-averaged horizontal velocity distribution highlighting the impingement region. Taken from Khayrullina et al. [3]	21
2.4	(a) Laboratory-scale experimental setup used by Frank and coworkers [4, 5], (b) shadowgraph image of an unstable air curtain installation highlighting fluid leakage from the modeled building envelope. Taken from Frank and Linden [4].	26
2.5	Real scale ACD installation: the curtain is installed above the doorway. Taken from Frank et al. [6].	28
2.6	Air curtain installation in the (a) warm room, (b) cold room, (c) warm room with intake grille placed in the floor. Contours of instantaneous temperature field: blue and red colors represent cold and warm fluids respectively. Velocity vectors overlaid to illustrate the flow field. Taken from Gonçalves et al. [7]	35
2.7	Iso-contours of coherent structures obtained by the Q-criterion at $t = 0.5632$ s. Taken from large-eddy simulation (LES) study of Moureh and Yataghene [8].	42

2.8	Organization of this thesis highlighting the addressal of applied and fundamental research questions posed.	47
3.1	Schematic of the computational setup used for RANS simulations. Indoor: light fluid (red), outdoor: heavy fluid (blue). Yellow face denotes plane of symmetry while pink and cyan boundaries represent domain inlet and outlet respectively.	56
3.2	A slice of the computational mesh used for the LES simulations. The mesh is coarsened by a factor of 8 and 2 in x and z directions respectively for visualization purpose.	60
3.3	(a) Schematic of the experimental setup at the instant before removing the lock-gate. The curtain fluid is same as that of the indoor fluid to create an NBAC. (b) An actual picture of the facility during the filling process. . . .	61
3.4	A mobile camera continuously monitors (30 Hz) the turbine flow meter that measures Q through the nozzle during an experiment.	62
3.5	Field of view of the DSLR camera for flow visualization.	65
3.6	Instrumentation for density measurement in the present study. Precision weighing balance (right) was employed in the preliminary stage in conjunction with a pycnometer and was later complemented with the density meter (left). The two measures differ within 5%.	67
3.7	(a) Variation of normalized centerline vertical velocity for RANS and LES simulations compared with the analytical solution for self-similar free jets [9] and PIV measurements [3]. (b) Cross-sectional normalized vertical velocity as a function of normalized cross-stream distance. Green and red symbols correspond to RANS and LES data at $\tilde{z} = 35$ respectively whereas black solid line denotes the hotwire measurements of [10]. The data in inset correspond to $\tilde{z} = 1$ and compares the inflow velocity profile with a uniform inlet flow shown as black.	72
3.8	Instantaneous buoyancy fields in the lock exchange flow (equivalent to the doorway without an air curtain installed) simulated using RANS and LES methodologies.	74
3.9	Pseudocolor plot of buoyancy distribution in the computational domain for (a) $D_m = 0$, (b) $D_m = 0.1$, (c) $D_m = 0.4$ and (d) $D_m = 0.8$ at $\tilde{t} \approx 8$ in the center plane.	76
3.10	Images from the dye visualization experiments showing (a) an unstable air curtain, and (b) an ACD in the stable regime. Heavy (outdoor) fluid is dyed green whereas the curtain fluid is marked using magenta dye.	76
3.11	Air curtain effectiveness as a function of deflection modulus for all the simulations reported in this study.	79
3.12	E vs. D_m curve obtained from the experiments and compared with the measurements of Jha <i>et al.</i> [11] and the previously plotted numerical data.	80

3.13	Temporal and spatial variations of the turbulent quantities associated with the TKE budget.	82
3.14	Transient variation of (a) turbulence production, (b) turbulent dissipation and (c) buoyancy production for various values of deflection modulus quantified using mesh III (LES).	85
4.1	An overview of the air curtain installation. Blue and orange colors represent a colder and a warmer fluid respectively.	88
4.2	Schematic of the experimental setup at the instant before removing the lock-gate. The curtain fluid is brine solution for the NBAC and aqueous solution of sugar for HAC.	92
4.3	Various additions and subtractions of salt mass from the dense fluid half during an experiment.	95
4.4	Control volume chosen for the formulation of the analytical model.	97
4.5	Snapshots recorded by the DSLR camera corresponding to experiment no. 12.	102
4.6	Estimates of the sealing effectiveness of heavy air curtain obtained from experiments and LES simulations. Blue and red dashed lines are approximate curve fits to the $E(D_m)$ data for $D_m \gtrsim 0.2$ for NBAC and HAC respectively.	103
4.7	Effectiveness estimated using 2D RANS simulations for varying S	105
4.8	Comparison of the mean centerline and RMS vertical velocity obtained from the LES simulation at different D_m to quantify the differences between an air curtain and an isothermal jet.	107
4.9	Comparison between the predictions of the analytical model and that of simulation (LES) data corresponding to a stable air curtain at $D_m = 0.4$	110
5.1	General schematic of (a) an impinging fountain in a uniform ambient, and (b) in an ambient providing a lateral forcing. Subscripts d and l corresponds to dense and light fluids respectively.	112
5.2	Computational schematic, shown at (a) initial time with boundary conditions, and a typical (b) impinging fountain depicting the induced curvature due to cross-stream buoyancy difference.	113
5.3	(a) Spatial distribution of $\frac{dl}{\eta}$ in the center plane evaluated on the finer grid. (b) Histogram representation of (a).	115
5.4	Schematic of the experimental setup at the instant before removing the lock-gate.	117
5.5	Density of aqueous salt solutions as a function of refractive index.	119
5.6	Nozzle 1: Comprising of series of holes ($\phi = 1.1$ mm) in a line fabricated on a milling machine.	121

5.7	Orthogonal views of the components of 2D nozzle obtained after CNC machining. All dimensions are in mm.	122
5.8	Isometric view of the 2D nozzle showing halves that are joined together to obtain the required jet cross-section. All dimensions are in mm.	123
5.9	Design components of the 2D nozzle.	124
5.10	Variation of the local exit thickness along the length of the nozzle.	125
5.11	Temporal evolution of normalised velocity at the central point of the domain. Data points in time windows corresponding to every 2 flow through times ($2T_f = 2H/w_0$) are colored differently and their short-time window average is shown using the horizontal black lines.	128
5.12	Short-time averaged fountain centreline.	128
5.13	Velocity statistics for the holed nozzle: (a) Normalised mean vertical velocity, and (b) Reynolds stress component, $\overline{u'w'}$, evaluated at different values of z/H and compared with hotwire measurements of Gutmark and Wygnanski [10] and DNS data of Klein et al. [12] for a non-buoyant jet.	129
5.14	(a) Normalised mean vertical velocity, and (b) Reynolds stress component, $\overline{u'w'}$, for the 2D nozzle evaluated at different values of z/H and compared with hotwire measurements of Gutmark and Wygnanski [10] and DNS data of Klein et al. [12] for a non-buoyant jet.	131
5.15	Temporal evolution of the normalised scalar field in the centerplane when viewed from the front, $C_j^*(x, W/2, z)$, and normalised vertical velocity as observed from the top, $w^*(x, y, H/2)$. Panels labeled as a , b , and c correspond to the cases NBJN ($Fr \rightarrow \infty$), PIF04N ($Fr = 28.4$, $L_j/H \approx 1.93$) and PIF01N ($Fr = 14.2$, $L_j/H \approx 0.77$) respectively while f and t implies front and top view in the their centerplane. The flow through time instants are: $t_1^* = 2.78$, $t_2^* = 5.56$, $t_3^* = 8.33$, $t_4^* = 11.11$, and $t_5^* = 13.89$ and the corresponding fields are shown in separate rows.	134
5.16	Time evolution of cases CF04N and CF01N, following the pseudocolor scheme as that in figure 5.15. The flow through time instants are: $t_1^* = 2.78$, $t_2^* = 5.56$, $t_3^* = 8.33$, $t_4^* = 11.11$, and $t_5^* = 13.89$ and the corresponding fields are shown in separate rows.	137
5.17	Spatiotemporal evolution of normalised spanwise vorticity, $\omega_y^*(x, W/2, z)$ computed on the fine grid for cases NBJN (panels a, d, and g), PIF04N (panels b, e, and h) and CF04N (panels c, f, and i). The flow through time instants are: $t_1^* = 0.5$ (left column), 1 (middle column) and 2 (right column) respectively.	140
5.18	(a) Pseudocolor spatiotemporal distribution of scalar near the wall, $C_j^*(x, 0.5W, 0.95H)$, for three cases: non-buoyant jet (top), forced fountain in homogeneous ambient (middle), and in crossflow (bottom). In (b), the normalized spreading distance after impingement on the non-buoyant half of the computational domain (i) and that in the buoyant half (ii) is shown.	142

5.19	Scaling of the dimensionless lateral spread, $\log\left(\frac{H+x_{sb}}{b_0}\right)$, in line fountains impinging in a homogeneous surrounding (cases PIF01N and PIF04N) as a function of their source Froude number, $\log(Fr_0)$	143
5.20	(a) Centerline trajectory for various numerical simulations; solid lines correspond to the respective central streamlines, (b) Mean local inclination angle, $\theta(z)$, for the impinging line fountains in crossflow, (c) Scaled representation of data in (a).	148
5.21	Case CF04N: (a) Normalised vertical and streamwise velocity along the fountain centreline. (b) The corresponding horizontal and stream-normal component. (c) Variation of RMS profiles associated with velocity components in (a) and (b).	150
5.22	Normalised mean streamwise velocity as a function of vertical distance obtained from experiments (lines) and numerical simulations (markers).	152
5.23	Spatial distribution of normalized mean velocity. Magenta lines represent the horizontal (x) cross-sections, whereas blue lines shows inclined (x_η) directions along which the investigation is performed in present study Circles and triangles represent the half-width and locations corresponding to twice the half-width.	155
5.24	Average half-width (a) and the ratio of jet half-widths on the buoyant and non-buoyant sides (b) obtained from the numerical simulations and compared with experimental estimates.	156
5.25	Mean streamwise velocity normalised with the local centreline velocity as a function of normalised cross-stream (x_η) distance.	158
5.26	Top row: Estimates of normalised RMS cross-stream velocity obtained from the simulations (left) and experiments (right). Bottom row shows the corresponding normalised RMS stream-normal velocity.	159
5.27	(a) Normalized mean velocity distribution overlaid with lines of constant normalized mean enstrophy and in (b), lines corresponding to $n\delta_{0.5}$ for $n = 1$ (black), 2 (blue) and 3 (red). Same lines are shown on the normalized mean enstrophy contour in (c) and (d). For isenstrophic lines, dashed (- -), solid (-) and dash-dotted (- ·) contours correspond to thresholds of 10^{-2} , 10^{-3} and 10^{-4} for normalised values of enstrophy.	162
5.28	Variation of volume flux (a) and momentum flux (b) along the stream direction, ξ . Quantities have been normalized with their respective source values.	166
5.29	Variation of integral length scale (a) and velocity scale (b). Quantities have been normalized with their respective source values.	167
5.30	(a) Integral entrainment coefficient obtained from experiments and simulations on non-buoyant jet for two different edge location consideration. (b) Values of α_r for all cases as a function of normalised vertical distance obtained from numerical datasets. Vertical lines denote the corresponding mean value.	171

6.1	Distribution of fluid particles (seed) at an initial time marking the outdoor fluid region projected on the $x - z$ plane. Seeding is coarsened for ease of visualization.	176
6.2	Transport mechanisms for fluid particles crossing the air curtain. (a) Gravity current (GC), (b) Entrainment-detrainment (ED), and (c) Entrainment-impingement (EI). Grey shaded regions represent the impingement zone.	178
6.3	Regions chosen for the conditional analysis of Lagrangian transport.	181
6.4	Temporal variation of crossing fraction resulting from Lagrangian transport from various spatial regions.	182
6.5	Probability distribution function associated with the tortuosity of fluid particle trajectories evaluated at $t^* = 5$	182
6.6	Probability distribution function associated with the tortuosity of fluid particle trajectories evaluated at $t^* = 20$	183
6.7	Crossing fraction, $X_f(t)$, plotted according to trajectory classification and compared with Eulerian estimate of fluid infiltration.	184
6.8	(a) Temporal evolution of the spatially averaged outdoor scalar in the indoor region, and (b) the corresponding scalar flux for various cases.	186
7.1	Pseudocolor contours of scalar concentration, C_j , mixed with the source fluid, showing asymmetric development of overturning billows on the two sides of air curtain ($D_m = 0.2$). Effect of density stratification on the evolution of vortical structures is also evident.	198

List of Tables

3.1	Different grids employed in the present work. Refinement is done in the central region for all the cases. N_{ACD} denotes the number of grid points spanning across the ACD nozzle whereas Δy and Δz denotes the spatial resolution in spanwise and vertical directions.	57
3.2	Simulations performed in the present study. In case numbering, the value of deflection modulus is stated after the first letter, D, whereas R corresponds to RANS and L denotes an LES simulation.	59
3.3	Various experiments conducted to characterize neutrally buoyant air curtains. Densities are in gm/cc whereas time is in seconds.	64
3.4	Validation metrics towards grid sensitivity study. Coefficient of discharge, C_D , and the constant of proportionality, k_1 , for the lock-exchange flow and the rates of jet centerline velocity decay, K_W , and its spread, K_δ	71
3.5	Estimates of centerline velocity decay rate (K_W) and spreading rate (K_δ) of the simulated planar jet. C_W and C_δ denotes the constants associated with the curve fit and are commonly referred to as virtual origins.	73
3.6	Coefficient of discharge, C_D , and the constant of proportionality, k_1 , for various uniform grids in a lock-exchange flow.	74
4.1	Various computations that were conducted for different values of deflection modulus, D_m , and the buoyancy ratio, S , where $S = 0$ corresponds to the neutrally buoyant air curtain.	90
4.2	The values of dimensionless parameters, Reynolds number (Re) and Richardson number (Ri), corresponding to heavy air curtains at various deflection modulus, D_m . Here, $g' = g \left(\frac{\rho_0 - \rho_d}{\rho_0} \right)$, and therefore, $Ri_{NBAC} = 0$	92
4.3	Various experiments conducted to characterize heavy air curtains. E and E' are calculated values of effectiveness based on density and conductivity respectively.	94

5.1	Large-eddy simulations conducted in the present chapter. Nomenclature: PIF denotes cases involving a uniform ambient, CF for fountains in cross-flow, NBJ corresponds to non-buoyant jet and GC stands for gravity current. Values with a [†] superscript implies that the corresponding density difference is calculated based on source and ambient fluid. In other cases, the lateral value of $\Delta\rho = \rho_d - \rho_l$ is used.	116
5.2	Experiments conducted in the present study.	120
5.3	Estimates of decay rate of centreline velocity (K_W), and the spread rate (K_δ) from experiments and numerical simulations. Experimentally measured quantities are written as $A \pm B$, where A is the ensemble average and B is the scatter associated across different repetitions, and should not be confused with the uncertainty in the reported values.	153
7.1	Primary measurements and their corresponding uncertainties.	208

List of symbols

ρ_0	Density of the air curtain fluid
ρ_l	Density of the light fluid
ρ_a	Density of the dense fluid
b_0	Exit thickness of the air curtain
w_0	Exit velocity of the air curtain
g	Acceleration due to gravity
H	Doorway height
D_m	Deflection modulus
E	Sealing effectiveness
g'	Reduced gravity
\mathbf{u}	Instantaneous velocity vector
$\bar{\mathbf{u}}$	Mean velocity vector
\mathbf{u}'	Fluctuating velocity vector
p	Instantaneous fluid pressure
\bar{p}	Mean fluid pressure
p'	Fluctuating fluid pressure
T	Fluid temperature
\mathbf{x}	Coordinate vector
t	Time
t^*	Dimensionless time
ν	Kinematic viscosity
κ	Thermal diffusivity
k	Turbulent kinetic energy
ϵ	Dissipation rate of k

τ_{ij}^R	Subgrid stress tensor
λ^R	Subgrid buoyancy flux
Re	Reynolds number
Fr	Froude number
V_r	Velocity ratio
S	Density difference ratio for heavy curtains
x_{sb}	Lateral spread on the buoyant side
x_{snb}	Lateral spread on the non-buoyant side
$\bar{\theta}$	Mean inclination of the air curtain
w_ξ	Streamwise velocity component
u_η	Streamnormal velocity component
K_W	Decay rate of centreline velocity
$\delta_{0.5}$	Jet halfwidth
K_δ	Spread rate of jet halfwidth
Q	Volume flux
M	Momentum flux
α_I	Integral entrainment coefficient
X_f	Particle crossing fraction
n_p^0	Initial number of seeding particles
$\tau(t)$	Tortuosity of the particle trajectory

List of abbreviations

HVAC	Heating, ventilation and air-conditioning
ACD	Air curtain device
RANS	Reynolds-averaged Navier-Stokes
LES	Large-eddy simulation
SOMAR	Stratified ocean model with adaptive refinement
PIV	Particle image velocimetry
NBAC	Neutrally buoyant air curtains
HAC	Heavy air curtains
TNTI	Turbulent/non-turbulent interface
IAQ	Indoor air quality
CFD	Computational fluid dynamics
LDA	Laser doppler anemometry
FDM	Finite difference method
RDC	Refrigerated display cabinets
ELF	External lateral flow
RNG	Renormalization group
RMS	Root mean square
CFL	Courant-Friedrichs-Lewy
LG	Lock gate
ST	Supply tank
DIT	Dye injection tank
LEF	Lock-exchange flow
GCI	Grid convergence index
HWA	Hot wire anemometry

KH	Kelvin-Helmholtz
TKE	Turbulent kinetic energy
NBJ	Non-buoyant jet
PIF	Plane impinging fountain
ODE	Ordinary differential equation
GC	Gravity current
ED	Entrainment-detrainment
EI	Entrainment-impingement
PLIF	Planar laser-induced fluorescence
